Imperial College London

Department of AERONAUTICS

Ammonia-Powered Regional Aircraft

Design Specification Document

GDP Group 04

apr.

Date-19/06/2023

Contents

1. Configuration Definition

The overall layout of the designed ammonia-powered regional aircraft with its key features are summarised in this section. The global aircraft layout with its key dimensions is shown in figure 1.

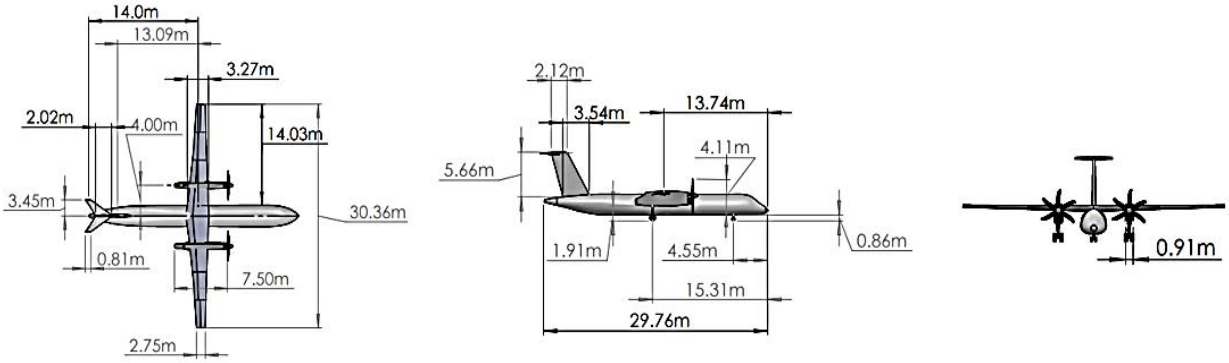

Figure 1. Global Aircraft Layout and Dimensions

The aircraft features a high wing with the ammonia fuel and fuel system stored in the wings, a nacelle mounted main landing gear, wing mounted turboprop engines and a T-tail. It can seat 48 passengers and 4 crew. It features a standard 2 x 1 seating configuration, with a main door in the front and a baggage bay in the rear sections of the fuselage. These features help in keeping the fuel system away from the passenger cabin, improve fuel efficiency and allow an experience passengers are familiar with. The aircraft has a wing loading of 3332 N/m^2 and a takeoff power-to-weight ratio of 23 W/N, obtained from its constraint diagram. The aircraft weights and the composition of its maximum takeoff weight obtained from its conceptual and preliminary design phases, are summarised in table 1 and figure 2 respectively. The weights estimation followed a progression of Class I, II and III estimates.

Table 1. Aircraft Weight Parameters

Parameter	Value
Empty weight (kg)	18601
Fuel weight (kg)	8320
Payload weight (kg)	5044
MTOW (kg)	31965
Mass growth factor	6.34

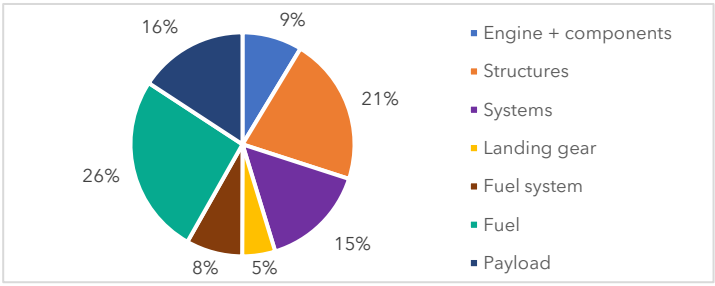

Figure 2. MTOW composition

The aircraft is designed for the mission profile depicted in figure 3. The aircraft's range is calculated as 1255 km, and its balanced field length is 1200 m. It has a takeoff distance of 1101.7 m, a landing distance of 1087 m and a one-engine-inoperative climb gradient of 7.36 %. Its specific excess power-performance is shown in figure 4.

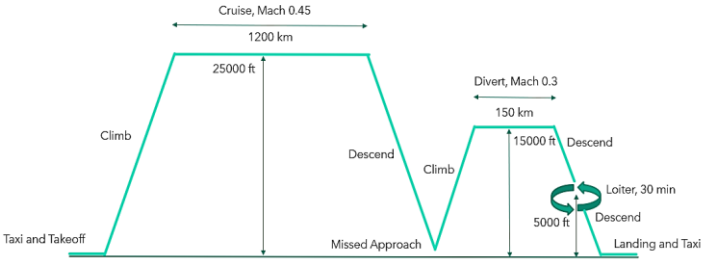

Figure 3. Aircraft Mission Profile

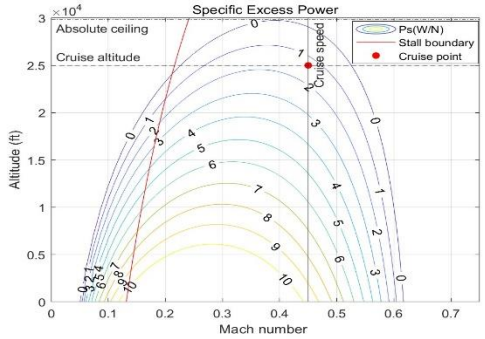

Figure 4. Specific Excess Power Plot

2. Propulsion Systems

2.1 Design Approach

There are two candidate engine designs for the aircraft: An electric motor system that uses fuel cell technology, or a direct ammonia combustion system that functions similar to existing turboprops, combusting ammonia or a

mixture of ammonia and hydrogen in the burner. As concluded in findings specified in the individual reports, the fuel cell technology was unfeasible as the system for purifying hydrogen could not meet hydrogen production rates required. Designing a direct ammonia combustion engine, it was noted that if ammonia could be catalytically cracked in a ratio that had similar burning properties to kerosene, minimal changes would have to be made to the engine design from the reference engine, the PW150. As a result of this, most of the design process was centred on creating and sizing a catalyst and heat extraction system that could convert ammonia into a suitable mixture of Hydrogen, Nitrogen and Ammonia, and analysing the engine propulsion properties. Much research was also conducted for different chemical combustion ratios and fuel staging.

2.2 Special Design Considerations

- Initially 680kW at 400˚C was required for the endothermic reaction in the catalyst, however, this was later reduced by injecting only 15% of the Ammonia into the catalytic converter for the pilot zone, while using pure Ammonia for the rest. The power requirement for the catalytic converter was reduced to 162kW, obtained from the exhaust.

- A fuel staging in the primary zone is considered to reduce NO_x emissions and ensure flame stability. Burning the fuel mixture near stoichiometric conditions in the pilot zone, while adjusting the fuel flow rate in the main zone if necessary.

- To minimise NOx emissions, ammonia is injected directly into the exhaust for reduction

- To maintain the temperature of the liquified ammonia at -50˚C, (50% safety factor), a cooling system integrated alongside Cryogel (FRAB) is utilised. Cooling system consists of a commercial refrigerated recirculating chiller (Lneya LT-65A1N), pumping propylene glycol coolant to the fuel tanks at varying mass flow rates.

2.3 Key Engine Parameters

Table 2. Key Engine Parameters

Spec	Value	Spec	Value
Fuel Mixture LHV	49kJ/kg	Insulation Thickness Inboard and Outboard	0.04m
Ammonia LHV	18.6kJ/kg	Outboard Tank Insulation Weight	220kg Per Wing
Fuel consumption rate	0.51kg/s	Inboard tank Insulation Weight	75kg Per Wing
TSFC	2.13E-05	$\dot{m}$,Coolant Outboard Tank	1.23kg/s
primary zone % of total air	15%	$\dot{m}$,Coolant Inboard tank	0.90kg/s
secondary zone % of total air	20%	Refrigerated Recirculating Chiller	Lneya LT-65A1N
cool linear walls % of total air	40%	Mass of Off the shelf Chiller	325kg per wing
dilution zone % of total air	25%	Catalyst Length	0.5m
Fuel to air ratio	0.0455	Catalyst Radius	0.078m
Stoichiometric Fuel to Air Ratio	0.1345	Catalyst + Fin Mass	40kg
Equivalence ratio	0.3382	Number of heating fins	40
Fin thickness	0.001m	Fin height	0.12m

3. Aerodynamic Design

The aerodynamic design process began by establishing the initial planform geometry. Following this, the airfoil was chosen through an optimization for both structural and aerodynamic performance. The design procedure was then divided into four primary categories:

Wing planform analysis & twist optimization: Using Prandtl's lifting line theory, the lift, drag and moment distributions across the span of the clean wing were evaluated. An optimization target towards elliptical lift

distribution was then set which geometrically twists the sectional airfoil at each span station to negate the change in C_l due to higher fidelity models on propeller wash, nacelle and fuselage effects. The optimization of twist reduced the induced drag from 137.24% of the induced drag for an elliptical distribution down to 117.65% of the induced drag for an elliptical distribution, yielding a 19.59% decrease in induced drag.

Drag prediction in different configurations: Zero-lift drag was estimated using the component build-up method while the induced drag was predicted by obtaining the lift coefficient of the wing and horizontal tailplane. This analysis was estimated for the Takeoff, Cruise, Approach and Landing at its current mass and true airspeed. Trim flight was assumed with C_{m_0}= 0 and thrust equal to drag. Parameters such as lift-to-drag ratio, range and thrust required were obtained from these estimations and then used to study the aerodynamic performance of alternative configurations. Table 4 shows a summary of the drag estimations and wing C_{D_0} compared with other methods such as VLM and the collocation method.

Integration of aerodynamic enhancements: Winglets were modelled in Tornado to quantify the increase in L/D but were later deemed unnecessary due to the already sufficient performance. Design and drag calculations were also competed for a wing fuselage fairing to reduce zero lift drag caused by their interference.

Numerical analysis using VLM and CFD: The Tornado vortex lattice framework was used to model the wing and its results compared with empirical and other computational methods. Some initial CFD was performed to verify drag calculations, e.g. drag on the nacelle. The wing was also modelled in OpenVSP and ran through a panel solver to assess the effects of thickness.

Table 3. Summary of planform geometry

Variables	R	λ	Span	S_{ref}	c/4 Sweep	Twist	Washout	Dihedral
Values	10	0.79	29.6 m	87.6 m	0˚	customized	-4.61˚	-1˚

Table 4. A summary of drag estimations and comparison of various methods for wing drag

Flight Configuration	**Takeoff**	**Cruise**	**Approach**	**Landing**
Aircraft Zero-Lift Drag Coefficient	0.0346	0.0174	0.0342	0.0939
Aircraft Induced Drag Coefficient	0.1936	0.0170	0.0737	0.1427
Total Drag Coefficient	0.2282	0.0344	0.1079	0.2366
Comparisons		Component Build Up	Tornado	Collocation
Wing Zero-Lift Drag		0.0047	0.0065	0.0052

4. Structural Design

Fuselage Design: To structurally size the fuselage, the 3 major loading cases (cruise at the ultimate load factor, one-engine inoperative and landing) were considered for loading analysis, which found the maximum shear force and bending moment to be 1.27 x 10^6 N and 2.52 x 10^6 Nm respectively. The skin, stringer, light frame configuration was optimised for mass by sweeping through all structurally viable configurations.

Table 5. Fuselage Structural Design Parameters

t_skin	No. of stringers	Stringer width	Light frame separation	Light frame height	Light frame base	Light frame thickness	Light frame shape
1.9 mm	96	1.7mm	35cm	5cm	10mm	1.5mm	Z Section

Fuel Tanks: The entirety of the fuel was placed in the wing. As the fuel tanks had to be insulated, a sandwich structure of aerofoil-insulation-fuel tank was made. The fuel tank was initially sized to have a wall thickness of 3mm however this will change in further iterations.

Material selection: Material selection was done by considering the most important parameters for each part of the aircraft and then analysed in CES software. After the analysis was concluded, it was decided that different types of aluminium alloys would be used: Al7068 T6511, Al7255 T7751, Al5182 H19, Al8019 and Al2024 T861.

Wing Design: The stringers and skin were designed using an iterative process focused on optimisation around creating a good design and minimising weight. The stringer and panels were analysed and varied at 3 stations along the span of the wing, at 4.6 m stations respectively. The ribs spacings were obtained, varying from 0.24 to 0.42 m. Further design of the ribs' thicknesses was conducted and values from 0.9 to 2.8 mm were obtained and integrated.

The spar is designed based on shear flow due to torque and shear force, which further optimised by adding vertical stiffeners. The maximum thickness for front and rear spar are 5 and 8mm respectively. D-section is designed based on double-cell closed-session tube, where the maximum thickness is determined to be 3.5 mm.

Tail Design: CFRP is the selected design material. It is assumed that the skin takes all the longitudinal load and the spar takes all the shear load on tailplane. An efficient design is achieved by alternating ply number and orientation.

Table 6. Empennage Composite Layup

Position (m)	Skin	Front Spar	Rear Spar
Horizontal Tail (HT)			
<0.69	(-45/90/0/45/0/90/0/0)s	(±45/90/±45/0/±45/0/90/±45)s	(±45/90/±45/0/±45/0/0/90/±45)s
<1.38	(-45/90/0/45/0/90/0/0)s	(±45/±45/0/±45/0/90/±45)s	(±45/±45/0/±45/0/90/±45)s
<2.07	(-45/90/45/0/90/0/0)s	(±45/±45/±45/0/90/±45)s	(±45/±45/0/±45/0/90/±45)s
<2.76	(-45/45/0/90/0)s	(±45/±45/0/90/±45)s	(±45/0/±45/90/±45)s
<3.45	(-45/45/90/0)s	(±45/0/90/±45)s	(±45/0/90/±45)s
Vertical Tail (VT)			
<1.42	(±45/90/0/0)s	(±45/90/90/0/0/±45)s	(±45/90/90/0/0/±45/0/±45)s
<2.12	(±45/90/0/0)s	(±45/90/90/0/0/±45)s	(±45/90/0/0/±45/0/±45)s
<2.83	(±45/90/0)s	(±45/90/0/0/±45)s	(±45/90/0/0/±45/0/±45)s
<3.54	(±45/90/0)s	(±45/90/0/0/±45)s	(±45/90/0/0/0/±45)s
<4.25	(±45/90/0)s	(±45/90/0/±45)s	(±45/90/0/0/±45)s
<5.66	(±45/90/0)s	(±45/90/0/±45)s	(±45/90/0/±45)s

5. Flight Dynamics and Control

The geometry of the empennage was determined with the goals of minimising drag and optimising static and dynamic stability.

Table 7. Empennage Geometry Parameters

Parameter	HT Value	VT Value
Airfoil	641012	661012
Aerodynamic centre from nose	28.5 m	25.7 m
Area	9.5 m^2	16 m^2
Aspect Ratio	5	2
Sweep at 1/4 chord	9.7	25.9
Taper Ratio	0.4	0.6
Root chord	2.02 m	3.54 m
Span	6.89 m	5.66 m
Dihedral	0	90
Twist	0	0

The geometry of the control surfaces was determined by analysing the aircraft under constraining flight conditions:

Table 8. Control Surfaces Geometry Parameters

Control Surface	Chord Ratio	Span Ratio	Deflection Range
Elevator	0.24	1.00	-30° to +10°
Aileron	0.376	3.9 meters	+-30°
Rudder	0.85	0.42	+-30°

The aircraft was found to be statically stable across all stages of flight, varying from 4% - 9% in the most constraining flight conditions. Theoretically, the elevator is capable of trimming the aircraft for the entire centre of gravity range at high-lift, however in power off stall flight tests, the elevator was found to lack authority. In power on stall flight tests, aileron authority was often reduced and sometimes roll control was lost entirely. Adding spoilerons would be a sensible design solution to maintain roll control at low speeds.

Hydro-electrostatic actuators were chosen for the primary control surfaces actuators and electro-mechanical as a redundancy. Results have indicated that the aircraft is dynamically and laterally stable. The aircraft is capable of banking 5 degrees in the full operational range of the mission profile, satisfying the requirement as stated in CFR § 25.149. All dynamical modes computed from a linearised state space model have suggested dynamical stability. While discrepancies exist between state space model solution and the flight simulation data, a general trend is observed and exhibit similar dynamical behaviour. The design of both the aileron and the rudder is carefully

tailored to meet the stringent requirements of OEI (One Engine Inoperative) conditions, cross-wind landing, and spin recovery, while simultaneously optimizing the geometry to enhance dynamic stability and improve handling quality.
This comprehensive design approach ensures that the aircraft maintains its control and stability under various operational scenarios. For lateral control, a combination of a Proportional-Integral (PI) controller and a Proportional-Derivative (PD) controller is employed. This inner-outer loop design enables the aircraft to effectively track specific trajectories while promptly responding to disturbances. The closed-loop frequency and time response analyses demonstrate the stability of the control system, ensuring reliable and predictable behavior in lateral maneuvers. In the longitudinal direction, a feedforward Proportional (P) controller is implemented to ensure a prompt response to trajectory signals. Additionally, two PID feedback controllers are employed for pitch attitude hold and velocity hold. This multi-controller setup enhances the robustness and ease of implementation of the longitudinal control system. The PID controllers contribute to maintaining the desired pitch attitude and airspeed, providing stability and control during various flight phases. The use of PID controllers in the longitudinal direction also facilitates precise trajectory tracking and prompt response to changes in flight conditions.
Overall, the meticulous design and implementation of the control systems for both lateral and longitudinal directions ensure that the aircraft exhibits rigorous control, stability, and responsiveness across a range of flight scenarios, contributing to enhanced safety and performance.

6. Infrastructure and Costs

To assess the feasibility of an ammonia powered aircraft, ammonia fuel production, transportation, and storage processes were evaluated and compared to existing kerosene-based aviation infrastructure. The primary factors considered were the cost, safety, emissions, and the impact on current operations. Ammonia is widely available, with global production approximately 70% of global fuel production. Production plants are widely available, and the production of ammonia can easily be scaled up for introduction into the aviation industry. The transportation of ammonia fuel from production site to storage facilities at the airport is relatively conventional involving the use of pipelines for large demand or more flexible fuel tankers for smaller demand situations. The transportation of ammonia fuel from production sites to aircraft stands for refuelling could use conventional refuelling trucks or a hydrant system. Due to risks involved a novel designated refuelling area is proposed. The turnaround time is comparable to similar kerosene powered aircraft. However, should a separate refuelling area be used, this would significantly increase the turnaround time. The aircraft can operate with existing ground support equipment apart from requiring constant ground power to cool the residual fuel in the fuel tanks. The taxiing and take-off/landing processes of ground operation require no significant modification. Ammonia will be stored in refrigerated cylindrical tanks in an area removed from the airport. Pipelines or fuel transport bowsers will be used to transport the fuel directly to the aircraft.

While ammonia is widely used and safety measures have already been established, the ammonia usage at airport poses new hazards. The risks are generally moderately high but with the right safety measures and regulations, it can be brought down to moderately low risk levels. The emissions savings would be highly dependent on the period of entry of ammonia-powered aircraft into commercial service and the production. When ammonia-powered aircraft enter commercial service in the future, it is likely that the ammonia used is mostly blue or green ammonia. A life-cycle CO_2 reduction from production to combustion of up to 92% can thus be achieved when making the switch from traditional kerosene-based jet fuel to ammonia fuel. There are several associated costs with the additional infrastructure can be separated into capital and operating costs. Key values are summarised in the following table:

Table 9. Summary of Key Values between Ammonia and Kerosene based Aircraft

Capital Costs (USD)	Operation Costs (USD)	Emissions	Turnaround Time and Configuration	Ground Operation	Safety
50 to 200 million higher	5 to 30 million higher	Up to 92% lower	Same time (37 minutes)	Additional GPU needed	Moderately higher risk

Based on the factors assessed above, an ammonia-based aviation industry with the design aircraft would achieve its primary goal of reducing carbon emissions to various degrees. However, this would come with cost and safety challenges. Any exposure or leakage could have catastrophic consequences. To overcome this, safeguards must be implemented both on ground infrastructure and on the aircraft. The analysis on fuel production, transportation and storage methods also show that a robust ground infrastructure is viable on the condition of large investment.